Robust Slip-Aware Fusion for Mobile Robots State Estimation

Ehsan Hashemi , *Member, IEEE*, Xingkang He , and Karl H. Johansson , *Fellow, IEEE*

Abstract—A novel robust and slip-aware speed estimation framework is developed and experimentally verified for mobile robot navigation by designing proprioceptive robust observers at each wheel. The observer for each corner is proved to be consistent, in the sense that it can provide an upper bound of the mean square estimation error (MSE) timely. Under proper conditions, the MSE is proved to be uniformly bounded. A covariance intersection fusion method is used to fuse the wheel-level estimates, such that the updated estimate remains consistent. The estimated slips at each wheel are then used for a robust consensus to improve the reliability of speed estimation in harsh and combined-slip scenarios. As confirmed by indoor and outdoor experiments under different surface conditions, the developed framework addresses state estimation challenges for mobile robots that experience uneven torque distribution or large slip. The novel proprioceptive observer can also be integrated with existing tightly-coupled visual-inertial navigation systems.

Index Terms—Sensor fusion, field robots, service robotics, autonomous agents.

I. INTRODUCTION

AUTONOMOUS mobile robots with augmented state estimation systems are revolutionizing accurate navigation for indoor and outdoor applications, such as field robots and autonomous driving [1]–[3]. Existing visual/LiDAR, or inertial based navigation designs are reaching their performance limits due to: vision-based navigation challenges in uncertain environments; disturbance and model mismatch challenges for LiDAR based localization; perceptually degraded conditions (e.g., due to dynamic objects) with wheel slip, which is common for field robots or indoor service robots with various payloads; or their growing complexities in presence of tire force nonlinearities and wheel slippage, impacting estimation error and update frequency in real-time [4]–[7]. Of the states of the wheeled mobile robot, information about the longitudinal and lateral speeds (i.e., slip ratio and sideslip) in the body frame is the significant contributor

in autonomous navigation [8], [9], for specific applications such as automated storage/retrieval in warehouses or indoor service robots that requires high accuracy of the robot position and orientation information [10], [11]. Speed and sideslip can be measured with Global Navigation Satellite System (GNSS). However, loss of reception and low bandwidth of commercial GNSS in indoor applications and urban canyons, as well as high-slip scenarios for GPS-inertial fusion schemes [12], are primary challenges for speed measurement in autonomous navigation. With limited visual/LiDAR/GNSS resources, two main approaches have been adopted in the literature for speed estimation robust to model uncertainties using the Inertial Measurement Units (IMU): kinematic- and wheel force-based approaches.

The former takes the form of stochastic observers [13], or visual-inertial state estimation [11], [14], [15] using accelerations/yaw rate from an IMU. A kinematic model, which relates perturbations to the mobile robot slipping is presented in [16] where slips are classified as multiplicative/additive inputs for trajectory tracking. Regular and event-based Kalman filter are designed in [17] to fuse IMU data and wheel odometry to estimate the speed and heading of mobile robots. A high-gain observer is designed in [18] to deal with unknown model parameters. The ego-motion is robustly estimated in [19] by employing a probabilistic model of the stereo sensor and IMU. Although kinematic-based methods do not require wheel longitudinal/lateral forces, they do not include wheel dynamics. This results in large localization errors (and drift) for high-slip cases during laterally excited scenarios.

The force-based approach uses optimization-based or stochastic observers and updates the estimated velocities with tire forces using Kalman, sliding mode, or nonlinear observers [20]. Uncertainties include surface friction and tire parameters, and render the navigation system susceptible to noises, specially for the wheel force saturation. A longitudinal slip estimator is proposed in [21] in an adaptive control strategy which employs neural network weight tuning. To deal with friction uncertainties, a parameter-varying observer is designed in [22] for slip estimation. Nonlinear observers are designed in [23] to estimate the speed and tires cornering stiffness, but the wheel dynamics has not been considered. Although force-based approaches provide better accuracy for slip estimation, they mostly need road-tire friction information and do not address large-slip scenarios, which are challenging for existing robot state estimators operating on various surface conditions. Hence, we propose and experimentally validate a speed (and slip) estimation framework robust to variations in model parameters

and surface conditions (in normal and high-slip scenarios) by developing a new inertial-tire model considering wheel and slip dynamics. The main contributions of the paper are summarized as:

- Designing a state estimation framework, which implements a robust proprioceptive observer at the wheel level, for autonomous navigation under a large range of wheel slippage;
- Developing a novel inertial-tire model for the proprioceptive observer which includes the wheel dynamics, does not require the road friction information, and integrates kinematic- and forces-based state observers robustly to bounded uncertainties in the model;
- Designing a robust fusion based on covariance intersection (CI) on wheel-level estimates, to improve the reliability of slip estimation in harsh and combined-slip scenarios.

The remainder of the paper is organized as follows: Section II presents the new model and wheel-level state estimator. Section III introduces the robust fusion framework for speed estimation. We investigate the performance of the approach in Section IV for experiments in normal and harsh high-slip scenarios on various surfaces. The conclusion is drawn at last.

II. WHEEL-LEVEL STATE ESTIMATION

In this section, we introduce an observer designed by using proprioceptive sensory data at each corner of the mobile robot.

A. Model Description

The longitudinal relative velocity $v_{rx}(t) = R_e \omega(t) - v_{xc}(t)$ and tire internal deflection state ξ of the average lumped Lu-Gre model [24], with the model description $\dot{\xi}(t) = v_{rx}(t) - (\kappa R_e \omega(t) + C_0)\xi(t)$, are used as states $x(t) = [\xi(t) \quad v_{rx}(t)]^\top$ at each corner. R_e is the effective tire rolling radius, $\omega(t) > 0$ is the wheel rotational speed which is physically bounded, κ is the normal force distribution coefficient, and v_{xc} is the longitudinal velocity in the tire coordinate system. The transient coefficient $C_0 := \frac{\sigma_0 |v_{rx}|}{\mu g(v_r)}$ includes the lateral rubber stiffness σ_0 and the road friction condition represented by $0.1 \leq \mu \leq 1$. The term $C_0 \xi$, which includes road friction and combined-slip characteristics of the model, is assumed to be part of the bounded uncertainty ϱ_ξ in the corner-based observer design. Relative longitudinal acceleration yields $\dot{v}_{rx} = R_e \dot{\omega} - \dot{v}_{xc} + \varrho_v$, where $\dot{v}_{xc}$ is the mapped longitudinal acceleration of the wheel's center obtained by the measured acceleration a_x and yaw rate r (by an IMU at the robot's Center of Gravity, CoG). The term ϱ_v is due to the model mismatch (i.e., uncertainties) in the relative longitudinal acceleration. The output is the normalized force in the LuGre model as $y := f_x = \sigma_0 \xi + \sigma_1 \dot{\xi} + \sigma_2 v_{rx}$ that can be obtained from the wheel dynamics $T - R_e F_x = I\dot{\omega}$ with T as the input torque at each robot corner [22]. Therefore, the augmented inertial-tire model at each corner $i \in \{\text{fL, fR, rL, rR}\}$ (for front-left, front-right, rear-left, and rear-right wheels) yields the following system, where the wheel speed $\omega : \mathbb{R}_{\geq 0} \to \mathcal{S}_p$ is a bounded time-varying parameter:

$$\dot{x}_i(t) = A_i(t)x_i(t) + Bu_i(t) + \varrho_i,$$
$$y_i(t) = C_i(t)x_i(t) + \bar{\varrho}_i, \tag{1}$$

in which $A_i(t) = \begin{bmatrix} -\kappa R_{e,i}\omega_i(t) & 1 \\ 0 & 0 \end{bmatrix}$, $B = [0 \quad 1]^\top$, $u_i(t) = R_{e,i}\dot{\omega}_i - \dot{v}_{xc,i}$, and $\varrho_i = [\varrho_{\xi,i} \quad \varrho_{v,i}]^\top$. The output matrix is $C_i(t) = [\sigma_0 - \kappa\sigma_1 R_{e,i}\omega_i(t) \quad \sigma_1 + \sigma_2]$ and $\bar{\varrho}_i = \sigma_1 \varrho_{\xi,i}$. Regarding the system uncertainties ϱ_i and $\bar{\varrho}_i$, we assume that $\mathbb{E}\{\varrho_i(t)\varrho_i^\top(t)\} \leq Q_i(t)$, $\mathbb{E}\{\bar{\varrho}_i(t)\bar{\varrho}_i^\top(t)\} \leq R_i(t)$. Note that the uncertainties could be colored, meaning that the uncertainties at different time instants may be correlated.

B. Wheel-Level Slip Estimation

We design a state observer estimator in this subsection to estimate the speed and longitudinal slip using the augmented inertial-tire model presented in (1), in presence of various slips at each tire. In this regard, we will prove consistency of the wheel-level observer (in the sense of uniformly bounded MSE). In order to deal with longitudinal slip at each wheel, the wheel-level observer (which is a Kalman-Bucy optimal variance estimator), is designed for estimation of relative velocities and wheel internal states:

$$\dot{\hat{x}}_i = A_i(t)\hat{x}_i + Bu_i(t) + K_i(t)(y_i(t) - C_i(t)\hat{x}_i(t)),$$

$$K_i(t) = \frac{\eta}{2} P_i(t) C_i^\top(t) R_i^{-1}(t)$$

$$\dot{P}_i(t) = A_i(t)P_i(t) + P_i(t)A_i(t)^\top + \eta P_i(t) + \frac{2}{\eta}Q_i(t)$$
$$- K_i(t)C_i(t)P_i(t), \tag{2}$$

where $\eta > 0$, K_i is the observer gain, and P_i is the error covariance. Let $\mathbf{I}$ be the identity matrix with proper dimensions, and Q_i, R_i are the process and measurement covariances. Assume that $\mathbb{E}\{(x_i(0) - \hat{x}_i(0))(x_i(0) - \hat{x}_i(0))^\top\} \leq P_i(0)$ that is valid since the fusion framework estimate the robot speed and wheel slips, which are consistent and do not experience *kidnapped* cases. Denoting the estimation error by $\tilde{x}_i(t) := x_i(t) - \hat{x}_i(t)$, we are able to provide a bound on the mean square error, i.e., $\mathbb{E}\{\tilde{x}_i \tilde{x}_i^\top\}$, in the following lemma.

Lemma 1: The mean square estimation error for the observer (2) is upper bounded, i.e., $\mathbb{E}\{\tilde{x}_i(t)\tilde{x}_i^\top(t)\} \leq P_i(t)$.

Proof: See Appendix A. □

Remark 1: The parameter-varying estimator (2) employs a reduced number of tire parameters (rubber stiffness and damping $\sigma_0, \sigma_1, \sigma_2$ and force distribution factor κ) which are independent of the road friction condition.

The following assumptions are provided for the proof of uniformly bounded mean square estimation error.

Assumption 1: There exist positive scalars β_1, α, α_2, β_2 and γ_0 such that

$$\alpha_2 \mathbf{I} \leq \int_t^{t+\gamma_0} \Phi_{t,\tau}\Phi_{t,\tau}^\top d\tau \leq \beta_2 \mathbf{I}, \quad \forall t \in [0, \infty),$$

$$\alpha_1 \mathbf{I} \leq \int_{t-\gamma_0}^t \Phi_{\tau,t}^\top C_i(\tau)^\top C_i(\tau)\Phi_{\tau,t} d\tau \leq \beta_1 \mathbf{I}, \forall t \in [\gamma_0, \infty),$$

where $\Phi_{t,\tau} \in \mathbb{R}^{n \times n}$ satisfies $\frac{\partial \Phi_{t,\tau}}{\partial t} = A_i(t)\Phi_{t,\tau}$, $\Phi_{\tau,\tau} = \mathbf{I}$

Assumption 2: There exist positive scalars α_3, β_3, α_4 and β_4 such that $\forall t \in [0, \infty)$,

$$\alpha_3 \mathbf{I} \leq R_i(t) \leq \beta_3 \mathbf{I}, \quad \alpha_4 \mathbf{I} \leq Q_i(t) \leq \beta_4 \mathbf{I}.$$

Theorem 1: The mean square estimation error is uniformly upper bounded, i.e., there is a constant matrix $\hat{P}_i \geq 0$, such that $E\{\tilde{x}_i(t)\tilde{x}_i^\top(t)\} \leq \hat{P}_i$.

Proof: Construct the following system

$$\begin{cases} \mathrm{d}\mathcal{X}_t &= \mathcal{A}_t\mathcal{X}_t\mathrm{d}t + \mathcal{B}_t\mathrm{d}\omega_t, \\ \mathrm{d}\mathcal{Y}_t &= C_t\mathcal{X}_t\mathrm{d}t + \mathcal{D}_t\mathrm{d}\omega_t, \end{cases} \quad (3)$$

where $\mathcal{A}_t = A_i(t) + \frac{\eta}{2}\mathbf{I}$, $\mathcal{B}_t\mathcal{B}_t^\top = \mathcal{Q}_t \triangleq \frac{2}{\eta}Q_i(t)$, $\mathcal{B}_t\mathcal{D}_t^\top = \mathbf{0}$ and $\mathcal{D}_t\mathcal{D}_t^\top = \mathcal{R}_t \triangleq \frac{2}{\eta}R_i(t)$, ω_t is the standard Wiener process. According to the theory of stochastic differential equation, the state $\mathcal{X}_t$ in the system (3) satisfies

$$\mathcal{X}_t = \Psi_{t,\tau}\mathcal{X}_\tau + \int_\tau^t \Psi_{t,\sigma}\mathcal{B}_\sigma\mathrm{d}\omega_\sigma, \quad (4)$$

where $\Psi_{t,\tau} = e^{\frac{\eta}{2}(t-\tau)}\Phi_{t,\tau}$. Denote $\mathcal{M}_{s,t} \triangleq \int_s^t \Psi_{\tau,t}^\top C_\tau^\top C_\tau \times \Psi_{\tau,t}\mathrm{d}\tau$, $\forall t \geq s$. Then, by Assumptions 1-2, for any $t \geq \gamma_0$, there is

$$\alpha_1 e^{-\eta\gamma_0}\mathbf{I} \leq \mathcal{M}_{t-\gamma_0,t} \leq \beta_1\mathbf{I}, \quad (5)$$

$$\int_{t-\gamma_0}^t \Psi_{t,\tau}\mathcal{Q}_\tau\Psi_{t,\tau}^\top\mathrm{d}\tau \leq e^{\eta\gamma_0}\beta_2\frac{2\beta_4}{\eta}\mathbf{I}. \quad (6)$$

In addition, for any $t \geq \gamma_0$, by the positive definiteness of $\mathcal{M}_{t-\gamma_0,t}$, a state estimate for the system (3) can be

$$\bar{\mathcal{X}}_t = \mathcal{M}_{t-\gamma_0,t}^{-1}\int_{t-\gamma_0}^t \Psi_{\tau,t}C_\tau^\top\mathrm{d}\mathcal{Y}_\tau. \quad (7)$$

By combining (4) and (7), we have the following error

$$\begin{aligned} \bar{\mathcal{E}}_t &\triangleq \mathcal{X}_t - \bar{\mathcal{X}}_t \\ &= \mathcal{M}_{t-\gamma_0,t}^{-1}\int_{t-\gamma_0}^t \Psi_{\tau,t}^\top C_\tau^\top C_\tau \Psi_{\tau,t}\mathrm{d}\tau\mathcal{X}_t \\ &\quad - \mathcal{M}_{t-\gamma_0,t}^{-1}\int_{t-\gamma_0}^t \Psi_{\tau,t}C_\tau^\top (C_\tau\mathcal{X}_\tau\mathrm{d}\tau + \mathcal{D}_\tau\mathrm{d}\omega_\tau) \\ &= \mathcal{M}_{t-\gamma_0,t}^{-1}\int_{t-\gamma_0}^t \mathcal{M}_{t-\gamma_0,\tau}\Psi_{t,\tau}\mathcal{B}_\tau\mathrm{d}\omega_\tau - \Psi_{\tau,t}C_\tau^\top\mathcal{D}_\tau\mathrm{d}\omega_\tau, \end{aligned} \quad (8)$$

where the last equality is obtained by exchanging the order of integration and replacing subscript σ by τ. It follows from (5), (6), (8), and Assumption 2 that

$$\begin{aligned} \mathbb{E}\{\bar{\mathcal{E}}_t\bar{\mathcal{E}}_t^\top\} &\leq \mathcal{M}_{t-\gamma_0,t}^{-1}\int_{t-\gamma_0}^t \Psi_{\tau,t}^\top C_\tau^\top \mathcal{R}_\tau C_\tau \Psi_{\tau,t}\mathrm{d}\tau\mathcal{M}_{t-\gamma_0,t}^{-1} \\ &\quad + \mathcal{M}_{t-\gamma_0,t}^{-1}\int_{t-\gamma_0}^t \mathcal{M}_{t-\gamma_0,\tau}\Psi_{t,\tau}\mathcal{Q}_\tau\Psi_{t,\tau}^\top\mathcal{M}_{t-\gamma_0,\tau}\mathrm{d}\tau\mathcal{M}_{t-\gamma_0,t}^{-1} \\ &\leq \left(n\beta_1\mathrm{tr}\left(\int_{t-\gamma_0}^t \Psi_{t,\tau}Q_\tau\Psi_{t,\tau}^\top\mathrm{d}\tau\right) + \frac{2\beta_3}{\eta}\right)\mathcal{M}_{t-\gamma_0,t}^{-1} \\ &\leq \hat{P}_1 \triangleq 2\frac{e^{\eta\gamma_0}\beta_3 + 4e^{2\eta\gamma_0}\beta_1\beta_2\beta_4}{\eta\alpha_1}\mathbf{I}. \end{aligned}$$

Obviously, the solution of Riccati equation in (2) is the optimal estimation error covariance matrix of system (3). Therefore,
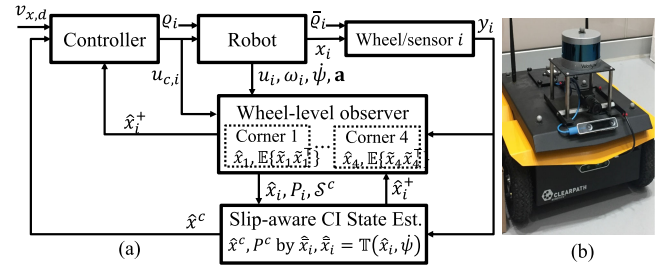

Fig. 1. (a) Slip-aware inertial-odometry architecture for robot state estimation (b) *Clearpath Robotics' Jackal* platform for experimental studies.

$P_i(t) \leq \mathrm{E}\{\bar{\mathcal{E}}_t\bar{\mathcal{E}}_t^\top\} \leq \hat{P}_1$ for any $t \geq \gamma_0$. Denote

$$\hat{P}_i \triangleq \max\left\{\hat{P}_1, \sup_{t\in[0,\gamma_0]} P_i(t)\right\}. \quad (9)$$

The conclusion follows from Lemma 1. □

The architecture of the slip-aware robot state estimator is shown in Fig. 1(a). The wheel-level observer utilizes u_i and measurements y_i to obtain state estimate $\hat{x}_i$ and set $\mathcal{S}^c$ for the CI-based fusion; the overall states $\hat{\bar{x}}_i$ is then used for the CI to obtain the estimate of the overall speed $\hat{v}_x$ (through $\hat{x}^c$) and to update the corner slip states $\hat{x}_i^+$. The mobile robot platform, which is used for experimental validation of the estimator on various surfaces, is shown in Fig. 1(b).

Remark 2: If the system has parameter uncertainties as

$$\begin{aligned} \dot{x}_i(t) &= (A_i(t) + \Delta A_i(t))\, x_i(t) + Bu_i(t) + \varrho_i, \\ y_i(t) &= (C_i(t) + \Delta C_i(t))\, x_i(t) + \bar{\varrho}_i, \end{aligned} \quad (10)$$

where $\Delta A_i(t)$ and $\Delta C_i(t)$ denote the uncertainties in the dynamics and measurements, respectively. Then, we rewrite (10) into the following expression

$$\begin{aligned} \dot{x}_i(t) &= A_i(t)x_i(t) + Bu_i(t) + \Delta A_i(t)x_i(t) + \varrho_i, \\ y_i(t) &= C_i(t)x_i(t) + \Delta C_i(t)x_i(t) + \bar{\varrho}_i. \end{aligned} \quad (11)$$

Then, the observer in (2) can still be used by enlarging $Q_i(t)$ and $R_i(t)$ such that

$$\mathbb{E}\{(\Delta A_i(t)x_i(t) + \varrho_i)(\Delta A_i(t)x_i(t) + \varrho_i)^\top (t)\} \leq Q_i(t)$$

$$\mathbb{E}\{(\Delta C_i(t)x_i(t) + \bar{\varrho}_i)(\Delta C_i(t)x_i(t) + \bar{\varrho}_i)^\top (t)\} \leq R_i(t).$$

As a result, the consistency in Lemma 1 still holds.

III. SLIP-AWARE INERTIAL ODOMETRY

The estimated states at the wheel level will be used in the CI fusion on $\hat{x}_i$ to estimate the speed in the body frame, and will be remapped to each robot's corner (wheel) for guidance control purposes (Fig. 2) of the four estimates.). Assume the discretization step on system (1) and estimator (2) is sufficiently small (i.e., $T_s = 20\text{ms}$ in real-time implementation for the test platform) such that the pair $(\hat{x}_i(k), P_i(k))$ inherits the property in *Lemma 1*: $\mathbb{E}\{\tilde{x}_i(k)\tilde{x}_i^T(k)\} \leq P_i(k)$, where $\tilde{x}_i(k) = \hat{x}_i(k) - x_i(k)$. The overall state satisfies the condition
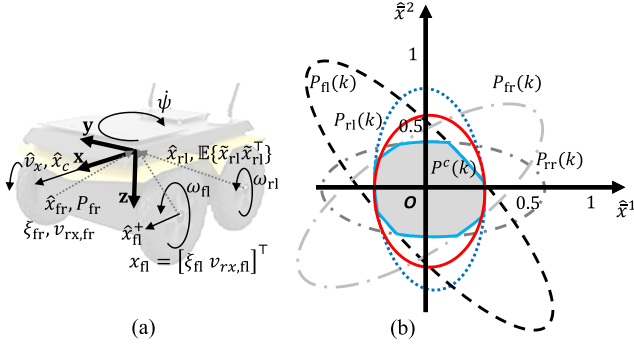
Fig. 2. (a) The body frame and states $\hat{x}_i$ from the augmented inertial-tire model; (b) Fusion of wheel-level estimates by CI.

$\bar{x}(k) = \mathbf{w} - x_i(k) + \bar{L}_i \frac{\dot{\psi}(k)}{2}$ where $\mathbf{w} = [R_e \omega_i(k)\ 0]^\top$, the parameter $\bar{L}_i$ represents the signed front/rear track widths (L_f, L_r) as $L_f := -\bar{L}_{\text{fL}} = \bar{L}_{\text{fR}}$ and $L_r := -\bar{L}_{\text{rL}} = \bar{L}_{\text{rR}}$, and the robot yaw rate measured at CoG is denoted by $\dot{\psi}(k)$ which is bounded and has zero-mean noise. Then, we are able to obtain the estimate of the overall state $\hat{\bar{x}}_i(k)$ at CoG at the k-th step by using the estimate of the local state $\hat{x}_i(k)$ transformed to the overall state:

$$\hat{\bar{x}}_i(k) = \mathbb{T}(\hat{x}_i(k), \dot{\psi}(k)) = \mathbf{w} - \hat{x}_i(k) + \bar{L}_i \frac{\dot{\psi}(k)}{2}. \quad (12)$$

Since the transformation is linear, it follows that

$$\mathbb{E}\{(\hat{\bar{x}}_i(k) - \bar{x}(k))(\hat{\bar{x}}_i(k) - \bar{x}(k))^T\} \leq P_i(k), \quad (13)$$

Then, we use the covariance intersection (shown in Fig. 2(b)) to fuse the estimates as in (14). In Fig. 2(b), each of the corners forms a dotted ellipsis. The solid red ellipsis, covering the common area of the wheel-level variances, is obtained through CI (i.e., $P^c(k), x^c(k)$). The CI estimates $\hat{x}^c(k)$, the speed of the robot in the body frame. Then, it is remapped to the corners for initialization of the local observer as $\hat{x}_i^+(k)$ for the next time step.

$$P^c(k) = \left(\sum_{i=1}^4 a_i P_i^{-1}(k) \right)^{-1},$$

$$\hat{x}^c(k) = \sum_{i=1}^4 a_i P^c(k) P_i^{-1}(k) \hat{\bar{x}}_i(k), \quad (14)$$

where $a_i > 0$. The optimal a_i that minimizes $\text{tr}(P^c)$ is obtained from $\min \text{tr}(P^c)$ such that $\sum_{i=1}^4 a_i = 1$. According to the consistency in (13) and the property of CI, it holds that

$$\mathbb{E}\{(\hat{x}_i^c(k) - \bar{x}(k))(\hat{x}_i^c(k) - \bar{x}(k))^T\} \leq P^c(k). \quad (15)$$

The slip-aware observer and fusion is described in Algorithm 1.

Remark 3: If the system has parameter uncertainties as in (10), the design of $Q_i(t)$ and $R_i(t)$ in Remark 2 ensures the local estimation consistency (13). Then the estimation consistency remains valid after applying the CI method, i.e., (15) holds in this case.

To deal with extreme slip conditions, the consensus leverages an adaptive set allocation strategy and excludes corners,

---

Algorithm 1: Slip-Aware State Estimation.

Initial. : Initial wheel-level slip/speed estimator covariances Q_i, P_i, S_i and estimate $\hat{x}_i(0)$

Output: v_x and corner slips λ_i in the body frame

while $k \geq 0$ **do**

1. Wheel-Level Slip Ratio Rates
   For each corner $i \in \mathcal{S}^w$, $\mathcal{S}^w := \{\text{fL, fR, rL, rR}\}$:
   i) Obtain slip rates: $u_i(k) \leftarrow R_e \dot{\omega}_i(k) - \dot{v}_{xc,i}(k)$;
   if $|\omega_i(k)| \leq \bar{\omega} \wedge \|\mathbf{a}\|_2 \leq \bar{a}$, $\mathbf{a} = [a_x, a_y]$ **then**
   $\quad \hat{x}_i(k) \leftarrow [\hat{x}_i(0)\ R_e \omega_i]^\top$;

   else
   2. Augmented State Observer
   i) Form $A_i(k), C_i(k)$, and $K_i(k)$;
   ii) Estimate wheel-level states $\hat{x}_i(k)$ by (2), where the MSE is bounded by
   $\hat{P}_i \triangleq \max\left\{\hat{P}_1, \sup_{t \in [0, \gamma_0]} P_i(k)\right\}$;

   end

   3. Adaptive Set Allocation
   if $|\dot{\omega}_i(k)| \geq \mu_{\dot{\omega}} \triangleq \frac{1}{n} \sum_{k-n+1}^k \dot{\omega}_i(k)$ **then**
   $\quad \mathcal{S}^c(k) \leftarrow \mathcal{S}^w \setminus \{i\}$;

   end

   4. Slip-Aware Consensus for Odometry
   if $\mathcal{S}^c(k) \neq \emptyset$ **then**
   i) Transform $(\hat{\xi}_i(k), \hat{v}_{rx,i}(k))$ to overall states $\hat{\bar{x}}_i(k) \leftarrow \mathbb{T}(\hat{x}_i(k), \dot{\psi}(k))$ by (12);
   ii) Use CI on estimates of overall states:
   $P^c(k) \leftarrow \text{CI}(P_i^{-1}(k))$;
   $\hat{x}^c(k) \leftarrow \sum_{i=1}^4 a_i P^c(k) P_i^{-1}(k) \hat{\bar{x}}_i(k)$;

   else
   $\quad \hat{x}^c(k) \leftarrow \hat{x}^c(k-1)$

   end

   i) Update states $\hat{x}_i^+(k) \leftarrow \mathbf{w} - \hat{x}^c(k) + \bar{L}_i \frac{\dot{\psi}(k)}{2}$ and $\lambda_i(k) = \frac{[0\ 1]\hat{x}_i^+(k)}{\min\{R_e \omega_i, v_{xc,i}\}}$;
   iii) Update Robot's speed $\hat{v}_x(k) \leftarrow [0\ 1]\hat{x}^c(k)$;

end

---

which exhibits large wheel rotational accelerations $\dot{\omega}_i(k)$ (i.e., $|\dot{\omega}_i(k)| \geq \mu_{\dot{\omega}}$ where $\mu_{\dot{\omega}} \triangleq \frac{1}{n} \sum_{k-n+1}^k \dot{\omega}_i(k), n = 4$), from the set on which covariance intersection (14) is utilized.

IV. EXPERIMENTAL RESULTS AND DISCUSSION

The computational efficiency and performance of the estimator (in real-time) is evaluated through a *Clearpath's Jackal* autonomous mobile robot. The tests are conducted in indoor/outdoor in various combined-slip scenarios in which the nonholonomic test platform experience slips at each tire. The performance of the developed consensus in extremely large-slip cases ($\lambda_i \geq 80\%$ at specific tires), which significantly affect the lateral stability of the robot, is also validated. The model parameters include wheels' moment of inertial $I_w = 1.5 \text{kgm}^2$, tire parameters $\sigma_0 = 67, \sigma_1 = 0.3, \sigma_2 = 0.005, \kappa = 12.7, R_e = 0.07$ identified by recursive least squares over actual wheel forces with the R^2 of 0.9 and RMS error of 7%. The model is discretized by step-invariant method, in which the discrete-time realization is approximated by $A_{i,k}^d k \triangleq \phi_{t_{k+1}, t_k}^{A_i} \approx e^{A_i(t_k)T_s}, B_{i,k}^d \triangleq$
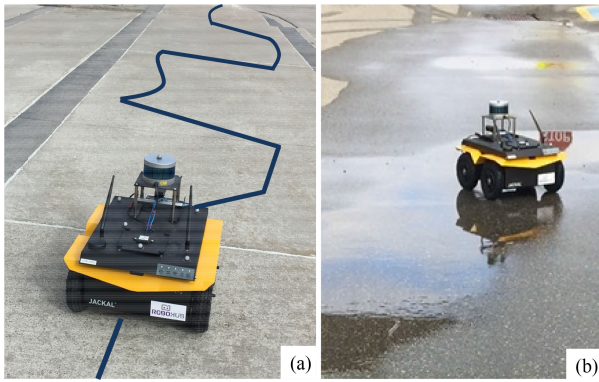
Fig. 3. (a) Robot's path for an obstacle avoidance (b) Cornering with large- and uneven-slip on varying surface friction conditions (i.e., dry and wet).
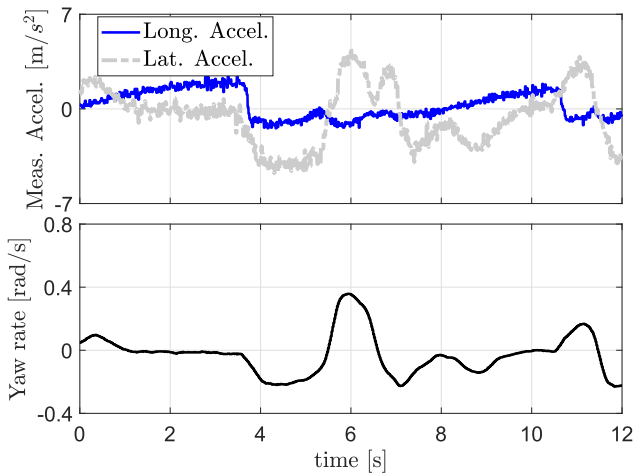

Fig. 4. Accelerations and yaw rate for obstacle avoidance at the force capacity.
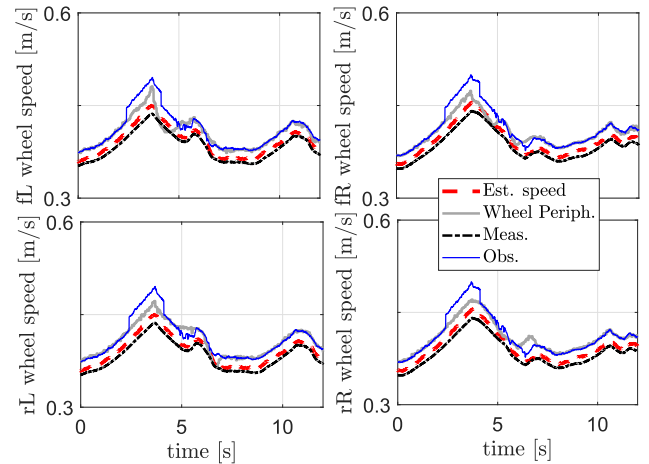

Fig. 5. Estimated speeds (by the slip-aware consensus) at each wheel in an obstacle avoidance at the capacity limit with several accelerated cornering.
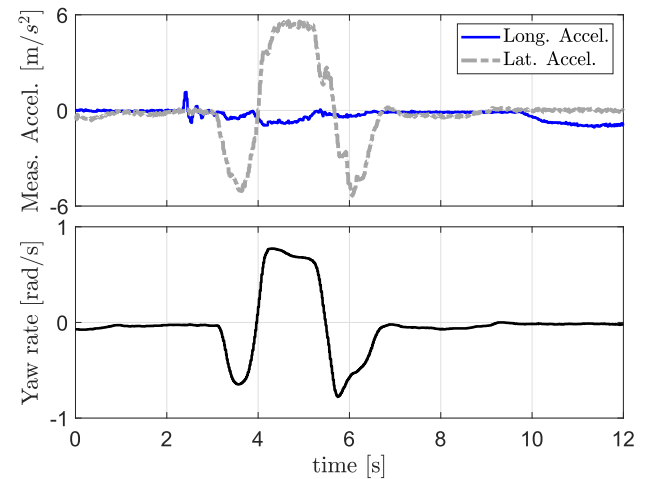

Fig. 6. Measured accelerations and yaw rate for navigation in outdoor (on asphalt) with combined-slip tire forces during cornering.

$\int_{t_k}^{t_{k+1}} \phi_{t_{k+1},\tau}^{A_i} B_i(\tau)d\tau \approx \int_{t_k}^{t_{k+1}} e^{A_i(t_k)(t_{k+1}-\tau)} d\tau . B_i(t_k)$, and $C_{i,k}^d = C_i(t_k)$, whereas $\phi_{t_l,t_j}^{A_i}$ is the state transition matrix, which can be expressed by the Peano-Baker series. The realization is assumed to not vary significantly in each interval $[t_k, t_{k+1}]$, which is valid for the platform and the estimator with the sampling time $T_s = 0.02s$.

A. Harsh Obstacle Avoidance At the Capacity Limit

The proposed estimator is validated in several obstacle avoidance scenarios (for which the quantitative results are provided at the end of this section) at the capacity limit in indoor/outdoor settings; we present the results of two scenarios in the following. Fig. 3(a) depicts the robot path for an obstacle avoidance, for which the the measured accelerations (shown in Fig. 4) confirm several cornering together with occasional longitudinal traction request (by the control system). The longitudinal speed estimation results are shown in Fig. 5, where the wheel peripheral speed denoted by "Wheel Periph." is obtained by multiplication of each wheel rotational speed ω_i and the effective rolling radius R_e. The ground truth "Meas.," and the estimated longitudinal speed by the developed slip-aware fusion (i.e., "Est. speed") are compared with the peripheral speed and a state-of-the-art approach [22]

which implements robust parameter-varying (LPV) observers, shown by "Obs.,"to address large-slip cases. The labeling for ground-truth and comparison method remains consistent in this section. One of main challenges for the existing kinematic- or wheel force-based state estimators is persistency of the wheel slip and tire force saturation that significantly increases model mismatch. As a result, the LPV approach has large estimation errors for long-term large slip conditions as can be seen between $2.5 < t < 4.5s$ in this test. This has been addressed in the proposed CI-based fusion that implements an adaptive set allocation strategy.

Another obstacle avoidance experiment, which includes deceleration during cornering (by the motion planner), is conducted in outdoor setting on asphalt. The measured lateral accelerations and yaw rate in Fig. 6 confirm simultaneous avoidance and deceleration between $t = 3.8$ and $4.7s$ and after $9.7s$. This results in a combined-slip tire force behaviour (during path tracking), which is challenging for existing wheel odometry-based or inertial-based navigation systems, but the
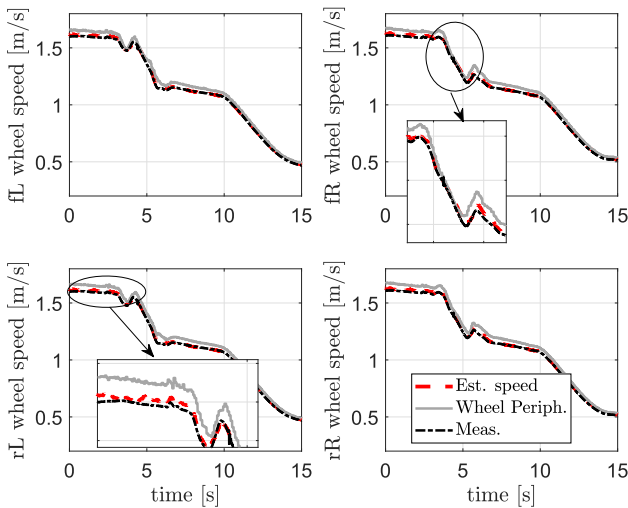
Fig. 7. Slip-aware consensus results for longitudinal speed/slip estimates in an obstacle avoidance with several deceleration during cornering on asphalt.

Fig. 9. Measured accelerations and yaw rate for a cornering with uneven slip due to different torque distribution.
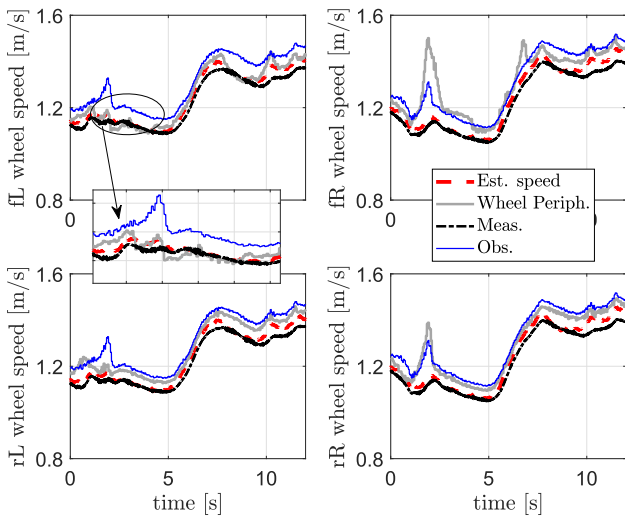

Fig. 8. Longitudinal speed estimates in a high-speed obstacle avoidance on gravel. The developed consensus outperforms the existing robust observer (i.e., Obs.) and handles high-slip cases at all wheels, between $t = 1$ and 3.2s.

Fig. 10. Longitudinal speed estimates in with uneven wheel slip on a slippery surface. The large front-right slip is handled by the slip-aware fusion.

estimated longitudinal speeds at each wheel are consistent and has good convergence as shown in Fig. 7. Another high-speed and combined-slip cornering scenario is conducted in outdoor on gravel, and the result are provided in Fig. 8, where the estimated longitudinal speeds at each wheel (in presence of several slip cases for all wheels due to trajectory tracking on gravel with extra traction requests) is compared with the ground truth and the LPV observer. The developed slip-aware CI-based estimator, which does not use any information on road surface friction, outperforms the LPV observer in terms of smaller estimation error and faster convergence.

B. Large- and Uneven-Slip Scenarios During Cornering

The performance of the robust consensus for uneven slip scenarios is evaluated in this subsection, where extremely large-slip
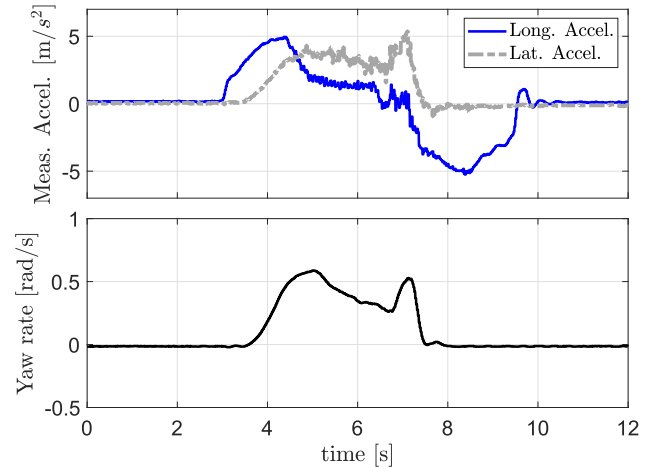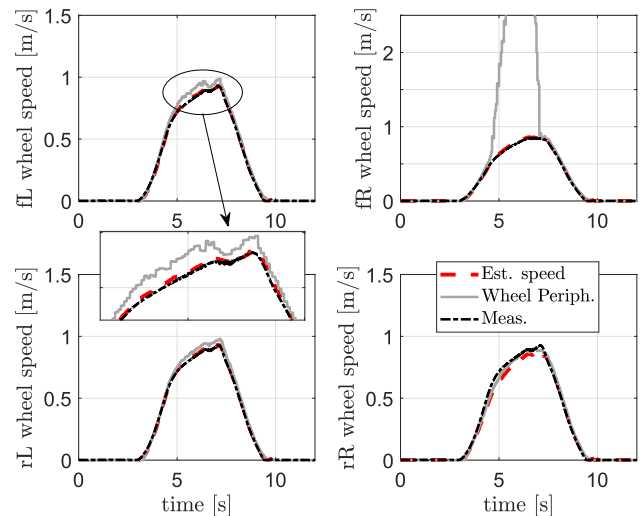
tests are conducted on slippery surfaces (as shown in Fig. 3(b)) Such cornering scenarios, with consequent load transfer, necessitates incorporating the wheel dynamics, as considered in the developed estimator as an augmented state. The following test includes uneven slip due to the varying surface friction condition and uneven *torque distribution*, which is used for skid steering. The measured lateral acceleration, which confirms motion at the limit of capacity on the wet surface, is provided in Fig. 9. The large wheel speed at the robot's front-right corner (from $t = 3.8$ to 7.6s) in Fig. 10, and simultaneous lateral acceleration up to the capacity of 5m/s^2 in Fig. 9, confirm combined-slip wheel forces, thus arduous characteristics of this test. The results presented in Fig. 10 confirm the effectiveness of the proposed estimation framework in addressing uneven and rapidly increasing wheel rotational speed due to uneven torque distribution.

Quantitative Results: Variations of the robot's speed estimation error RMS are depicted in Fig. 11, for various road surface
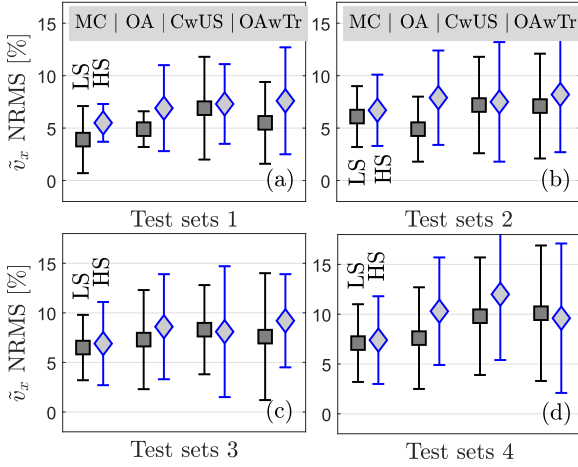
Fig. 11. RMSE distribution for the developed estimator on various surfaces and actuation system configurations in high-speed (HS) and low-speed (LS) maneuvers. Rear-wheel drive on high-grip and gravel are studied in (a) and (b), respectively. (c) and (d) show the results for the all-wheel actuation.
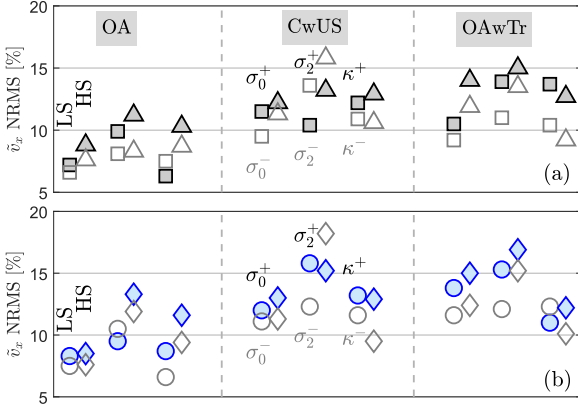

Fig. 12. Performance under model parameter changes for low- and high-speed; the superscripts $+$ and $-$ on parameters $\sigma_{0,2}, \kappa$ resembles $\pm30\%$ changes. (a) rear-wheel actuation (b) all-wheel electrically actuated powertrain.

conditions in indoor/outdoor settings and actuation system configurations for high-speed (HS) and low-speed (LS) maneuvers. The mean values are depicted by bold (black and red) lines and the plot bounds represent σ. Different tests include mild cornering/turning (MC), obstacle avoidance (OA), cornering with uneven slips at each wheel (CwUS), and obstacle avoidance with additional longitudinal acceleration requested by the motion planner during cornering (OAwTr). For the mobile robot's low-speed ($v_x \leq 0.6$ m/s) and high-speed ($0.6 < v_x \leq 2$ m/s) cases, 15 different tests have been conducted for each scenario with various traction requests. They are studied for four different cases: The Test set 1 includes the above mentioned scenarios on high-grip surfaces in indoor with the rear-wheel drive actuation; Test set 2 denotes the same actuation configuration, but on gravel and slippery surface; other two cases are for scenarios with all-wheel drive powertrain system, but on different surfaces, i.e., indoor in Test set 3 and gravel in Test set 4.

The robustness of the developed estimator to changes in model parameters, and with all- and rear-actuated power train systems is also studied and provided in Fig 12. It is compared in terms

of $\mathbb{E}\{\tilde{v}_x \tilde{v}_x^\top\}$ for changes in the model parameters, i.e., rubber stiffness/damping σ_0, σ_2 and load factor κ. 30% changes in σ_2 has larger effect on estimation error compared with changes in σ_0, κ. The RMSE is bounded by 17.4% (using the robust wheel-level observer and adaptive set allocation for the fusion) for the arduous cases of accelerated obstacle avoidance in high speed with all-wheel actuation. The overall average of RMSE are 6.2% and 8.8% for all low- and high-speed tests, respectively, on various surfaces.

V. CONCLUSION

A state and slip estimation framework, which implements a robust observer at the wheel level, was developed and validated for navigation of autonomous mobile robots experiencing wheel slippage in indoor and outdoor (e.g., asphalt, gravel) settings. Integrating kinematic- and forces-based slip estimators, the developed framework includes the wheel dynamics, to improve the reliability of inertial odometry in harsh/combined-slip scenarios, and does not require road surface friction information. Addressing slip estimation challenges for robots that experience uneven torque distribution at each tire, the developed estimator exhibited good performance on various surface frictions. The performance of the designed slip-aware observer was compared with a state-of-the-art robust parameter-varying observer that uses a switching mechanism to address various surface conditions. The slip-aware observer outperformed the LPV observer, in terms of smaller estimation error and faster convergence, implementing an adaptive set allocation strategy to exclude corners with large wheel rotational accelerations for the CI. The robustness of the estimator to large variations in model parameters (up to 30%) is also studied, and confirmed RMSE less than 18% for both all- and rear-actuated power train systems. As the future work, the novel proprioceptive observer can also be integrated with existing tightly-coupled visual-inertial navigation systems to address localization and odometry challenges under large-slip conditions.

APPENDIX A
PROOF OF LEMMA 1

It follows from (1) and (2) that the error satisfies

$$\dot{\tilde{x}}_i(t) = (A_i(t) - K_i(t)C_i(t))\,\tilde{x}_i(t) + \varrho_i(t) - K_i(t)\bar{\varrho}_i(t)$$

Then, the derivative of the mean square estimation error yields

$$\frac{\mathrm{d}\mathbb{E}\left\{\tilde{x}_i(t)\tilde{x}_i^\top(t)\right\}}{\mathrm{d}t} = \mathbb{E}\left\{\frac{\mathrm{d}\tilde{x}_i(t)\tilde{x}_i^\top(t)}{\mathrm{d}t}\right\}$$

$$= \mathbb{E}\left\{\dot{\tilde{x}}_i(t)\tilde{x}_i^\top(t) + \tilde{x}_i(t)\dot{\tilde{x}}_i^\top(t)\right\}$$

$$= (A_i(t) - K_i(t)C_i(t))\,\mathbb{E}\left\{\tilde{x}_i(t)\tilde{x}_i^\top(t)\right\}$$

$$+ \mathbb{E}\left\{\tilde{x}_i(t)\tilde{x}_i^\top(t)\right\}(A_i(t) - K_i(t)C_i(t))^\top$$

$$+ \mathbb{E}\left\{ (\varrho_i(t) - K_i(t)\bar{\varrho}_i(t))\, \tilde{x}_i^\top(t) \right.$$

$$\left. + \tilde{x}_i(t)\, (\varrho_i(t) - K_i(t)\bar{\varrho}_i(t))^\top \right\}$$

$$\leq (A_i(t) - K_i(t)C_i(t))\, \mathbb{E}\left\{ \tilde{x}_i(t)\tilde{x}_i^\top(t) \right\}$$

$$+ \mathbb{E}\left\{ \tilde{x}_i(t)\tilde{x}_i^\top(t) \right\} (A_i(t) - K_i(t)C_i(t))^\top + \eta\, \mathbb{E}\left\{ \tilde{x}_i(t)\tilde{x}_i^\top(t) \right\}$$

$$+ \frac{1}{\eta}\left(2Q_i(t) + 2K_i(t)R_i(t)K_i^\top(t) \right),$$

where $\eta > 0$. Denoting $\mathcal{A}_i(t) \triangleq A_i(t) - K_i(t)C_i(t) + \frac{\eta}{2}\mathbf{I}$, $\mathcal{P}_i(t) \triangleq P_i(t) - \mathbb{E}\{\tilde{x}_i(t)\tilde{x}_i^\top(t)\}$, and $\mathcal{Q}_i(t) \triangleq \eta\,\mathbb{E}\{\tilde{x}_i(t)\tilde{x}_i^\top(t)\} + \frac{1}{\eta}(2Q_i(t) + 2K_i(t)R_i(t)K_i^\top(t)) - \mathbb{E}\{(\varrho_i(t) - K_i(t)\bar{\varrho}_i(t)) \tilde{x}^\top(t) + \tilde{x}(t)(\varrho_i(t) - K_i(t)\bar{\varrho}_i(t))^\top\}$. Then, we can verify that $\mathcal{P}_i(0) \geq \mathbf{0}$, $\mathcal{Q}_i(t) \geq \mathbf{0}$. Therefore, $\mathcal{P}_i(t)$ satisfies the following Sylvester equation:

$$\dot{\mathcal{P}}_i(t) = \mathcal{A}_i(t)\mathcal{P}_i(t) + \mathcal{P}_i(t)\mathcal{A}_i^\top(t) + \mathcal{Q}_i(t),$$

which has a unique solution [25, Corollary 1.1.6] given as

$$\mathcal{P}_i(t) = \mathcal{V}_i(t,0)\mathcal{P}_i(0)\mathcal{V}_i^\top(t,0)$$

$$+ \int_0^t \mathcal{V}_i(t,\tau)\mathcal{Q}(\tau)\mathcal{V}_i^\top(t,\tau)\mathrm{d}\tau, \qquad (A2)$$

where $\mathcal{V}_i(t,\tau)$ satisfies $\frac{\partial \mathcal{V}_i(t,\tau)}{\partial t} = \mathcal{A}_i(t)\mathcal{V}_i(t,\tau)$, $\mathcal{V}_i(\tau,\tau) = \mathbf{I}$. From (A2), $\mathcal{P}_i(t)$ is semi-definite at each time t, leading to the conclusion of this lemma. $\qquad \square$

References

[1] R. Lenain, B. Thuilot, C. Cariou, and P. Martinet, "Mixed kinematic and dynamic sideslip angle observer for accurate control of fast off-road mobile robots," *J. Field Robot.*, vol. 27, no. 2, pp. 181–196, 2010.

[2] P. Yang, R. A. Freeman, and K. M. Lynch, "Multi-agent coordination by decentralized estimation and control," *IEEE Trans. Autom. Control*, vol. 53, no. 11, pp. 2480–2496, Dec. 2008.

[3] E. Hashemi, X. He, and K. H. Johansson, "A dynamical game approach for integrated stabilization and path tracking for autonomous vehicles," in *Proc. Amer. Control Conf.*, 2020, pp. 4108–4113.

[4] T. K. Marks, A. Howard, M. Bajracharya, G. W. Cottrell, and L. H. Matthies, "Gamma-SLAM: Visual SLAM in unstructured environments using variance grid maps," *J. Field Robot.*, vol. 26, no. 1, pp. 26–51, 2009.

[5] W. Hess, D. Kohler, H. Rapp, and D. Andor, "Real-time loop closure in 2D LIDAR SLAM," in *Proc. IEEE Int. Conf. Robot. Automat.*, 2016, pp. 1271–1278.

[6] T. Shan and B. Englot, "LeGO-LOAM: Lightweight and ground-optimized lidar odometry and mapping on variable terrain," in *Proc. IEEE/RSJ Int. Conf. Intell. Robots Syst.*, 2018, pp. 4758–4765.

[7] Y. Su, T. Wang, S. Shao, C. Yao, and Z. Wang, "GR-LOAM: LiDAR-based sensor fusion SLAM for ground robots on complex terrain," *Robot. Auton. Syst.*, vol. 140, 2021, Art. no. 103759.

[8] K. D. Do, Z.-P. Jiang, and J. Pan, "A global output-feedback controller for simultaneous tracking and stabilization of unicycle-type mobile robots," *IEEE Trans. Robot. Automat.*, vol. 20, no. 3, pp. 589–594, Jun. 2004.

[9] Y. Tian and N. Sarkar, "Control of a mobile robot subject to wheel slip," *J. Intell. Robotic Syst.*, vol. 74, no. 3, pp. 915–929, 2014.

[10] H.-Y. Chung, C.-C. Hou, and Y.-S. Chen, "Indoor intelligent mobile robot localization using fuzzy compensation and filter to fuse the data of gyroscope and magnetometer," *IEEE Trans. Ind. Electron.*, vol. 62, no. 10, pp. 6436–6447, Oct. 2015.

[11] S. Zhou, Z. Liu, C. Suo, H. Wang, H. Zhao, and Y.-H. Liu, "Vision-based dynamic control of car-like mobile robots," in *Proc. Int. Conf. Robot. Automat.*, 2019, pp. 6631–6636.

[12] K. Berntorp, "Joint wheel-slip and vehicle-motion estimation based on inertial, GPS, and wheel-speed sensors," *IEEE Trans. Control Syst. Technol.*, vol. 24, no. 3, pp. 1020–1027, May 2016.

[13] D. Selmanaj, M. Corno, G. Panzani, and S. M. Savaresi, "Vehicle sideslip estimation: A kinematic based approach," *Control Eng. Pract.*, vol. 67, pp. 1–12, 2017.

[14] V. Kubelka, L. Oswald, F. Pomerleau, F. Colas, T. Svoboda, and M. Reinstein, "Robust data fusion of multimodal sensory information for mobile robots," *J. Field Robot.*, vol. 32, no. 4, pp. 447–473, 2015.

[15] Q. Fan, B. Sun, Y. Sun, Y. Wu, and X. Zhuang, "Data fusion for indoor mobile robot positioning based on tightly coupled INS/UWB," *J. Navigation*, vol. 70, no. 5, 2017, Art. no. 1079.

[16] D. Wang and C. B. Low, "Modeling and analysis of skidding and slipping in wheeled mobile robots: Control design perspective," *IEEE Trans. Robot.*, vol. 24, no. 3, pp. 676–687, Jun. 2008.

[17] L. Marín, M. Vallés, Á Soriano, Á Valera, and P. Albertos, "Multi sensor fusion framework for indoor-outdoor localization of limited resource mobile robots," *Sensors*, vol. 13, no. 10, pp. 14133–14160, 2013.

[18] J. Huang, C. Wen, W. Wang, and Z.-P. Jiang, "Adaptive output feedback tracking control of a nonholonomic mobile robot," *Automatica*, vol. 50, no. 3, pp. 821–831, 2014.

[19] S. Omari, M. Bloesch, P. Gohl, and R. Siegwart, "Dense visual-inertial navigation system for mobile robots," in *Proc. IEEE Int. Conf. Robot. Automat.*, 2015, pp. 2634–2640.

[20] K. Nam, S. Oh, H. Fujimoto, and Y. Hori, "Estimation of sideslip and roll angles of electric vehicles using lateral tire force sensors through RLS and Kalman filter approaches," *IEEE Trans. Ind. Electron.*, vol. 60, no. 3, pp. 988–1000, Mar. 2013.

[21] H. Gao, X. Song, L. Ding, K. Xia, N. Li, and Z. Deng, "Adaptive motion control of wheeled mobile robot with unknown slippage," *Int. J. Control*, vol. 87, no. 8, pp. 1513–1522, 2014.

[22] E. Hashemi, S. Khosravani, A. Khajepour, A. Kasaiezadeh, S.-K. Chen, and B. Litkouhi, "Longitudinal vehicle state estimation using nonlinear and parameter-varying observers," *Mechatronics*, vol. 43, pp. 28–39, 2017.

[23] M. Fnadi, F. Plumet, and F. Benamar, "Nonlinear tire cornering stiffness observer for a double steering off-road mobile robot," in *Proc. Int. Conf. Robot. Automat.*, 2019, pp. 7529–7534.

[24] C. Canudas-de Wit, P. Tsiotras, E. Velenis, M. B. Gissinger, and G. Gissinger, "Dynamic Friction Models for Road/Tire Longitudinal Interaction," *Veh. System Dyn.*, vol. 39, pp. 189–226, 2003.

[25] H. Abou-Kandil, G. Freiling, V. Ionescu, and G. Jank, *Matrix Riccati equations in control and systems theory*. Basel, Switzerland: Birkhäuser, 2012.